

# Multilayer neutron stars with scalar mesons crossing term

Sebastian Kubis\* and Włodzimierz Wójcik

*Institute of Physics, Cracow University of Technology, Podchorążych 1, 30-084 Kraków, Poland*

Noemi Zabari

*Henryk Niewodniczański Institute of Nuclear Physics,*

*Polish Academy of Sciences,*

*Radzikowskiego 152, 31-342 Kraków, Poland*

It is shown that recently proposed RMF model with  $\sigma$  and  $\delta$  meson interaction agrees with the observational data and presents an interesting structure with phase transition in the outer part of neutron star core.

## I. INTRODUCTION

The internal structure of neutron stars (NS) is one of the most enigmatic subjects of nuclear astrophysics. The latest observation of the neutron-star merger, associated with gravitational waves detection, in August 2017 (Advanced LIGO/Virgo), revealed details on the mass and radius of neutron star determination. The event is known as GW170817 [1]. The estimations coming from this event have made the constraints on the equation of state (EOS) of nuclear matter by simultaneous determination of mass and radius of the newly born star. Precise mass measurements, however, without any information about stellar radius, come from rotating neutron star. Neutron star of the mass  $1.97 \pm 0.04 M_{\odot}$  (PSR J1614-2230) [2] and  $2.01 \pm 0.04 M_{\odot}$  (PSR J0348-0432) [3] has been reported in a binary system with a white dwarf. In 2018, the pulsar of the mass  $2.27 \pm 0.17 M_{\odot}$  (PSR J2215-5135) was identified using Fermi Large Area Telescope (Fermi LAT) by spectral lines analysis [4]. A feasible way to obtain maximum masses of the neutron star bigger than two solar masses is to retain befittingly stiff EOS. However, typical stiff EOS makes star less compact [5] which would be in contradiction to the radius estimation coming from GW170817. The typical soft EOS gives relatively smaller radius but might never reach the mass above  $2 M_{\odot}$ . In order to reconcile those two opposite tendencies, we propose a model giving the EOS, which is soft in low density (slightly above  $n_0$ ) and stiff at higher densities relevant for the inner part of the NS core.

In this paper, we show the EOS results for the model, which includes the  $\sigma - \delta$  meson crossing term. Modification of this type have been recently proposed and analyzed, see [6, 7]. The calculations are performed in the framework of the relativistic mean field (RMF) theory. The inclusion of such types of interactions leads to supersoft symmetry energy behavior and slope values that are consistent with most recent studies of nuclear matter properties. Here, we show results for the neutron stars that utterly conform to the mass and radius constraints mentioned above.

## II. MODEL

The base of the RMF theory gives adequate Lagrangian, which includes nucleons interacting through the exchange of four mesons. Two isoscalar mesons  $\sigma, \omega$  and two isovector  $\rho, \delta$  mesons. In this work, the proposed Lagrangian is enriched by a new kind of meson-meson interaction e.i. the  $\sigma - \delta$  meson crossing term [6].

Here, we are limiting the demonstration of the model only to the most relevant parts. Due to the inclusion of  $\sigma - \delta$  meson interaction, the corresponding part  $-\tilde{g}_{\alpha}\sigma^{\alpha}\vec{\delta}^2$  is added to the Lagrangian. The  $\alpha$  exponent distinguishes between two types of meson-meson interactions:  $\alpha = 1$  for linear and  $\alpha = 2$  for quadratic ones. This term modifies the equation of motion and leads to an additional contribution to the total energy density of matter

$$\epsilon_{\sigma\delta} = \tilde{g}_{\alpha}\sigma^{\alpha}\delta^2, \quad (1)$$

where  $\delta$  denotes mean value of the third component of the  $\vec{\delta}$  field. In the framework of RMF, for the considered model, there are seven free model parameters represented by the following coupling constants  $C_{\sigma}, C_{\omega}, C_{\rho}, C_{\delta}, b, c$  and  $g_{\alpha}$ . In the model parametrization, it is more convenient to use  $g_{\alpha} = \frac{\tilde{g}_{\alpha}}{4g_{\sigma}^{\alpha}g_{\delta}^2}$  instead of  $\tilde{g}_{\alpha}$ , where  $g_{\sigma}$  and  $g_{\delta}$  are meson-nucleon coupling constants appearing in the standard RMF Lagrangian. For more details we refer to the work [6]. Isoscalar sector consist of  $C_{\sigma}, C_{\omega}, b$ , and  $c$  coupling constants which values are attained to reproduce the symmetric nuclear matter. In our calculations we use  $n_0 = 0.16 \text{ fm}^{-3}$ ,  $B = -16 \text{ MeV}$  and  $K = 230 \text{ MeV}$ . We set the value of constant  $C_{\sigma}$  to be 11 MeV that gives sufficiently stiff EOS which is compatible with observations of PSR J2215-5135 and PSR J0740-6620. In the isovector sector,  $C_{\rho}, C_{\delta}$  and  $g_{\alpha}$  constants are chosen to obtain symmetry energy at saturation  $S_2(n_0) = 30 \text{ MeV}$  and acceptable value of the symmetry energy slope  $L = 3n_0 \frac{dS_2}{dn}|_{n_0}$ . Recent experimental data suggest a rather low slope, in the range between 40 and 80 MeV. Such low values are obtained as a result of the crossing term Eq.(1), if and only if  $\tilde{g}_{\alpha}$  (and the same  $g_{\alpha}$ ) takes negative values. Moreover, it was found that in model family with quadratic coupling, the phase transition at the low-density region emerges and leads

\* skubis@pk.edu.pl

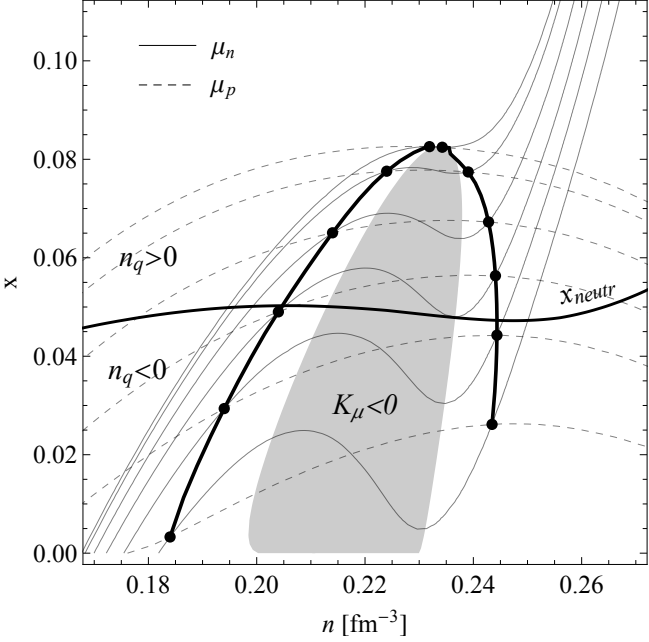


FIG. 1. Phase coexistence diagram for the model with quadratic interaction  $\alpha = 2$  and  $C_\delta^2 = 3.5 \text{ fm}^2$ . The thick line is the binodal curve with marked points being in chemical and mechanical equilibrium. The gray area denotes unstable phases - the spinodal region.

to a characteristic softening of the EOS. Whereas in the model family with linear coupling, the phase transition does not occur.

For a given nuclear model, we build the EOS of nuclear matter in  $\beta$ -equilibrium. The chemical potentials of each particle species satisfy the  $\beta$ -equilibrium equality

$$\mu_e = \mu_\mu = \mu_n - \mu_p, \quad (2)$$

where  $n, p, e, \mu$  stand for neutrons, protons, electrons and muons respectively. In order to control the slope value  $L$ , we manipulate the constant  $C_\delta$  while  $g_\alpha$  is fixed as it is shown in Table I - the higher  $C_\delta$  the lower value of the slope. A performed analysis revealed the occurrence of phase transition for high enough  $C_\delta$ . Indeed, such models appear to have negative values of incompressibility  $K_\mu$ , which signals a split into a two-phase system for the densities where  $K_\mu < 0$  emerges. The quantity

$$K_\mu = \left( \frac{\partial P}{\partial n} \right)_\mu \quad (3)$$

represents incompressibility under constant chemical potential of charge ( $\mu \equiv \mu_e = \mu_\mu$ ). It is the proper quantity to determine the region where the system ceases to be stable against charge fluctuations and has to split into two phases with opposite charge density [8]. The coexistence of those two phases takes place when their pressures and chemical potentials for particles being present in both

phases are equal to each other:

$$\begin{aligned} P(n_I, x_I) &= P(n_{II}, x_{II}) \\ \mu_i(n_I, x_I) &= \mu_i(n_{II}, x_{II}) \quad , \quad i = n, p, e. \end{aligned} \quad (4)$$

These equations, called Gibbs conditions, ensure the mechanical and chemical equilibrium between phases. They lead to the so-called Gibbs construction, which is shown on the proton fraction versus density diagram, Fig. 1. The spinodal region, marked with a gray area, represents the points where incompressibility is negative. Therein no stable phase arises. The Gibbs conditions Eqs. (4) are fulfilled for pairs of points for which  $\mu_p$  and  $\mu_n$ -contours intersect on the  $n-x$  space. These points form the curve called the binodal line. In the Fig.1, the line labeled  $x_{neutr}$  represents the locally neutral phase. Above that line all phases are positive ( $n_q > 0$ ). Below, they are negative ( $n_q < 0$ ). Global charge neutrality assures only points for phases with opposite charge may coexist in the real system. The global neutrality of the system determines the volume proportion between phases expressed by the equation

$$w(n_p^{(I)} - n_e^{(I)} - n_\mu^{(I)}) + (1-w)(n_p^{(II)} - n_e^{(II)} - n_\mu^{(II)}) = 0, \quad (5)$$

where  $w$  is the volume fraction occupied by the I-st phase,  $w = V^{(I)}/(V^{(I)} + V^{(II)})$ . The Gibbs conditions Eq.(4) and global charge neutrality Eq.(5) allow the finding of the region of phase space where two separated phases occur and uniquely determine the equation of state, e.i. the pressure versus energy density relation,  $P(\varepsilon)$ . It is worth noting that the phase separation appears for the quadratic interaction model with the most plausible value of slope  $L$ . For presented model with  $C_\delta^2 = 3.5 \text{ fm}^2$  and  $\alpha = 2$ , the slope is  $L = 55.4 \text{ MeV}$ . Albeit even lower values might be obtained for higher  $C_\delta^2$ . The phase separation usually leads to the softening of the EOS in comparison to the one-phase system. This phenomenon is well visible in Fig.2 at which a set of EOSs for different nuclear models is shown. The phase separation dramatically changes the slope of the  $P(\rho)$  relation for the coupling  $C_\delta^2$  exceeding  $3.0 \text{ fm}^2$ , which corresponds to the slope  $L$  smaller than  $68 \text{ MeV}$ . The derivative of the pressure with respect to density determines the sound velocity in the matter

$$v_s = \sqrt{\frac{\partial P}{\partial \rho}}. \quad (6)$$

In the lower panel in Fig.2 the sound speed is shown in a moderate range of densities. The sudden decrease of  $v_s$  corresponds to the phase transition region in which the speed of sound drops to around  $10^{-3}c$ .

### III. MULTILAYER NEUTRON STARS

The set of EOSs was constructed for the quadratic model for the  $C_\delta^2$  coupling within  $1.0$  to  $3.8 \text{ fm}^2$ . The

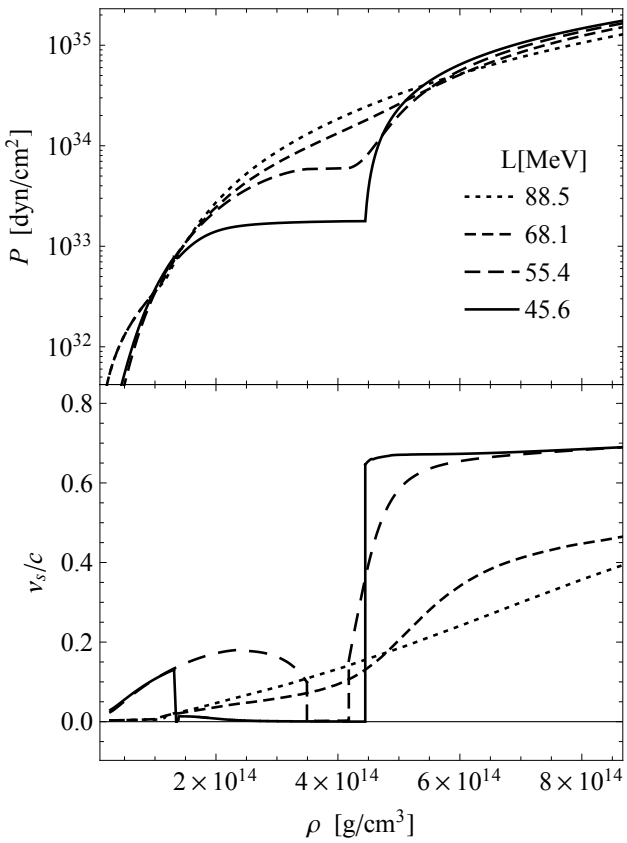


FIG. 2. The EOS and speed of sound for four different  $C_\delta^2$  couplings. Corresponding symmetry energy slope  $L$  are given in the legend.

corresponding values of the symmetry energy slope  $L$  are from 88.5 to 45.6 MeV. The proposed nuclear RMF model does not cover the region of very low densities, where the neutron star crust is formed. For the crust, the Sly4 model was used [9, 10]. The joining of crustal EOS and the EOS for the core is carried out at the point where their pressure and density are equal.

The structure of non-rotating NS is obtained by implementing given EOSs into Tolman-Oppenheimer-Volkoff (TOV) equations

$$P'(r) = -G(\epsilon(r) + P(r)) \frac{m(r) + 4\pi r^3 P(r)}{r(r - 2Gm(r))}, \quad (7)$$

$$m'(r) = 4\pi r^2 \epsilon(r),$$

where  $P$  and  $\epsilon$  pressure and energy density,  $m(r)$  is the gravitational mass (in units of energy) confined inside a sphere with radial coordinate  $r$ . The TOV equations reveal the nontrivial structure of star for the EOS with phase transition. The matter in the region of phase separation resembles the structure of inner crust - clusters with high proton fraction immersed in low proton environment or pure neutron matter and has solid-state

properties. Such a layer is separated from the actual star crust by a thin layer of homogeneous liquid matter. Concluding, the star includes the four different layers, two solid-like and two liquid ones. In Fig. 3 the subsequent layers with different properties are shown. Such a multilayer structure of neutron star requires further analysis in the context of rotational and vibrational properties. The solid-like internal layer should somehow manifest in the pulsar glitching or precession.

The fundamental relation between stellar parameters is the mass-radius relation. The  $M$ - $R$  relation for various  $C_\delta$  couplings is presented in Fig. 4.

For all considered couplings, the maximum mass is well above  $2 M_\odot$ , which is consistent with most recent observational data [2–4]. In particular, the models with  $L$  below 60 MeV are in the best agreement with the most massive pulsar PSR J0740+6620. As the observations of binary systems allowing for determining the mass of the neutron stars well enough, the precise measurements of stellar radius of a star with a known mass are still not attainable. Promising results were derived from the GW signal coming from the binary NS merger [1]. These results suggest a rather small radius of the star, which indicates soft EOS. However, typical soft EOSs lead to  $M_{max}$  lower than those for the most massive PSR. A specific EOS is required to find a balance between these two opposite facts. It should have different behavior in different ranges of density. The stiffness of the EOS at higher densities controls the maximum mass of a star, whereas at lower densities (closer to the crust) refers to the stellar radius. The results clearly show that considered models, with scalar-scalar meson interactions, make the EOS softer at moderate densities and stiffer at higher densities. This type of EOS comes from a specific form of the symmetry energy being very soft at a lower density region. This effect is most visible for the quadratic coupling model with  $L$  around 50 MeV. It was already shown by Fattoyev *et al.* [11] that soft symmetry energy

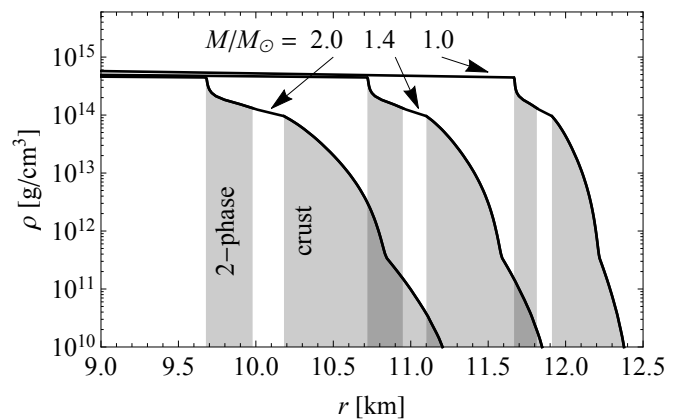


FIG. 3. The density profiles for different stellar masses for the model with  $L = 45.6$  MeV. The gray color indicates the solid-like structures.

is favorable regarding the results of GW170817. It was concluded from the analysis of the tidal deformability of binary components during the merging. The tidal deformability is sensitive to the compactness ( $M/R$ ) of a star and thus it is possible to find upper bound for the radius for a given mass. Another constraint for the stellar radius comes from the threshold mass for the prompt collapse to the black hole after the merging. Bauswein et al. [12] inferred that radius of a star with  $M = 1.6M_{\odot}$  cannot be smaller than 10.7 km. Both, upper and lower boundaries for the radius are shown in the Fig. 4. As one may see, the EOS for all  $L$  are placed within the allowable region. However, the models with  $L < 60$  MeV have the  $M_{max}$  being in better agreement with the present constraints from PSR mass measurement. The mass-radius relation for the EOSs with phase transition shows characteristic bending. For masses smaller than  $0.5M_{\odot}$  the stellar radius decreases with mass. For such low masses, the central density is located in the two-phase region where the EOS is very soft. When the stellar mass is greater, the central density enters into a homogeneous matter region where the EOS becomes much stiffer. Gravitation is no longer able to compress the matter in the core, and the further increase of the star mass causes an increase of the star radius. In this paper, we also show the influence of  $\sigma$ - $\delta$  meson interactions on the URCA process in  $npe\mu$  matter. The direct URCA process plays a crucial role in the cooling history of a of a neutron star. Applying

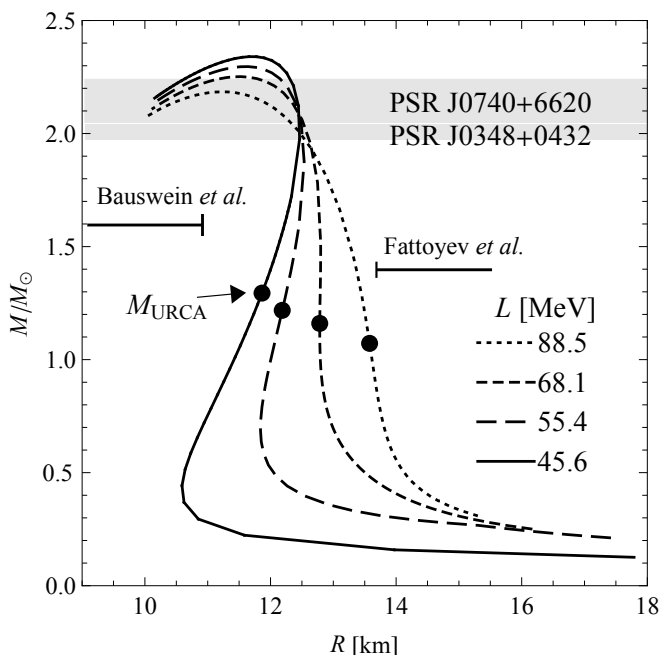


FIG. 4. Mass-radius profiles for various  $C_{\delta}^2$  corresponding to different  $L$ . The gray bands indicate the observed masses with their uncertainties. The horizontal segments present a region of forbidden values of radius from GW180718 analysis.

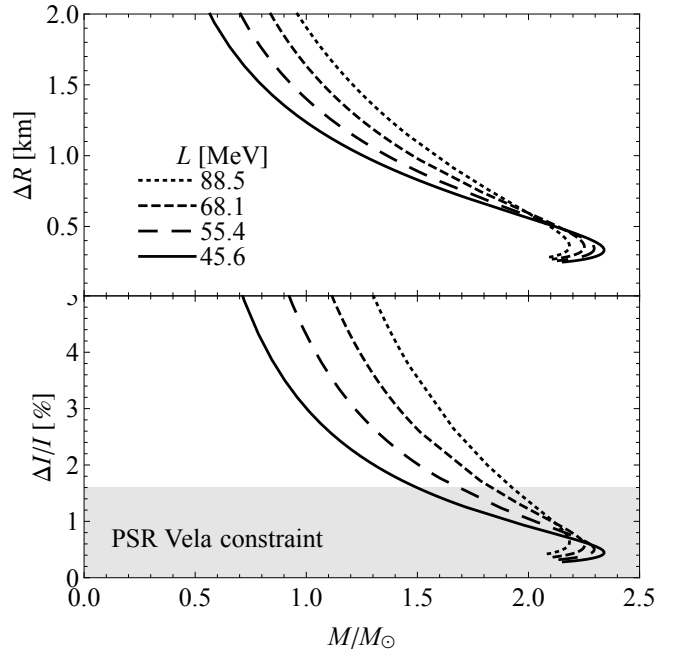


FIG. 5. The crust thickness and crustal moment of inertia as a function of stellar mass for different nuclear models.

dURCA threshold given by Eq.(8)

$$\left( x - \left( (1-x)^{1/3} - x^{1/3} \right)^3 \right)^{2/3} = \left( (1-x)^{1/3} - x^{1/3} \right)^2 - \left( \frac{m_{\mu}}{(3\pi^2 n)^{1/3}} \right)^2, \quad (8)$$

the  $x^{urca}$  and corresponding  $n^{urca}$  is found. In Fig. 4 the mass of a stars with the central density exceeding the threshold  $n^{urca}$  are indicated. A recent analysis of the cooling story of transient system MXB 1659-29 [13] strongly suggests the presence of rapid cooling of a neutron star core via the direct URCA. The direct URCA is only allowed when the symmetry energy increasing with the density sufficiently fast. In our model family, the symmetry energy dependence is the opposite. More than that, it may decrease with the density [6]. However, this behavior changes at some point, and again, the symmetry energy rapidly increases, making the proton fraction sufficiently large to ensure dURCA. That is why the critical stellar masses for dURCA (Fig. 4) are still in the typical range of neutron star masses.

Other parameters describing neutron star properties are associated with their crust. These are the crust thickness  $\Delta R$  and the crustal fraction of the total moment of inertia  $\Delta I/I$ . They have particular significance due to the possibility of their reliable observational evaluation from thermal relaxation of the crust and pulsar glitches [14]. A glitch phenomenon is a sudden increase in rotational frequencies that many pulsars exhibit. Their analysis based on the average rate of angular momentum

TABLE I. Basic neutron star properties for quadratic model family

$C_\delta^2$ [fm $^2$ ]	1.0	3.0	3.5	3.8
$L$ [MeV]	88.5	68.1	55.4	45.6
$M_{\max}/M_\odot$	2.18	2.25	2.27	2.34
$R_{\max}$ [km]	11.23	11.51	11.61	11.71
$n_c^{\max}$ [fm $^{-3}$ ]	1.001	0.932	0.896	0.865
$n_{\text{urca}}$ [fm $^{-3}$ ]	0.315	0.358	0.364	0.360
$M_{\text{urca}}/M_\odot$	1.07	1.16	1.22	1.29

transfer between the superfluid component and the crust [15] allows for estimating the crustal moment of inertia compared to the total moment of inertia of a star. Thus, the glitching phenomenon validates the crust-core transition being of particular importance. The more recent study of cumulative angular momentum transfer of Vela pulsar [16] points out that crust should encompass more than 1.6% of the total moment of inertia. The total moment of inertia  $I$  and its crustal fraction  $\Delta I$  have been computed using the formulas given in [17].

The total moment of inertia  $I$  and its crustal fraction  $\Delta I$  has been computed using the formulas given in [17]. The results are shown in the Figure 5. A promising method for simultaneous measurement of the mass and radius of a neutron star are based on observations of the quiescent mode in the low mass X-ray binaries [18]. Precise measurement of  $M$  and  $R$  are still out of the reach. The uncertainties for both of these quantities are quite significant. However, combined results from many observed LMXB shows an interesting tendency that observed stellar radius increases with mass [19]. This kind of relation between radius and mass is typical for EOS

being soft in the low-density region and becoming stiffer at higher density. Such EOS is achieved in our model for low value of the symmetry energy slope  $L$ , see Fig. 4.

#### IV. SUMMARY

In this work, we have shown the properties of neutron stars obtained in the framework of the recently proposed RMF model of nuclear interactions where the scalar mesons crossing term was applied [6]. Thanks to this new type of coupling, the symmetry energy slope  $L$  may reach sufficiently low values, as terrestrial experiments results from heavy-ion collisions suggest. Simultaneously, the model leads to the neutron stars which properties are in agreement with the most recent observational data concerning the NS masses and radii. Although not so convincing, the cooling data suggests that fast cooling by direct URCA cycle is present in neutron stars. Typically, the low values of symmetry energy block the URCA cycle by the low proton abundance in the NS core. It makes, therefore, the fast cooling questionable. However, the proposed model has interesting properties that, despite low symmetry energy slope, can still achieve proton fraction sufficiently large to ensure the presence of the direct URCA for stars with typical mass.

An additional outcome of the scalar meson couplings leads to phase separation in the outer part of the NS core. One may expect that nuclear matter with separated phases will acquire the solid-state properties. The presence of such secondary crust in the NS interior would have interesting implications requiring further analysis.

---

[1] B. Abbott *et al.* [LIGO Scientific and Virgo], Phys. Rev. Lett. **119** 161101 (2017).

[2] P. B. Demorest, T. Pennucci, S. M. Ransom, M. S. E. Roberts, and J. W. T. Hessels, Nature **467**, 1081 (2010).

[3] J. Antoniadis *et al.*, Science **340**, 6131 (2013).

[4] M. Linares, T. Shahbaz, and J. Casares, Astrophys. J. **859**, 54 (2018).

[5] M. Oertel, M. Hempel, T. Klähn, and S. Typel, Rev. Mod. Phys. **89**, 015007 (2017).

[6] N. Zabari, S. Kubis, and W. Wójcik, Phys. Rev. C **99** 035209 (2019).

[7] N. Zabari, S. Kubis, and W. Wójcik, Phys. Rev. C **100** 015808 (2019).

[8] S. Kubis, Phys. Rev. C **76**, 025801 (2007).

[9] E. Chabanat, P. Bonche, P. Haensel, J. Meyer and R. Schaeffer, Nucl. Phys. A **635**, 231 (1998).

[10] F. Douchin and P. Haensel, Astron. Astrophys. **380**, 151 (2001).

[11] F. Fattoyev, J. Piekarewicz, and C. Horowitz, Phys. Rev. Lett. **120** 172702 (2018).

[12] A. Bauswein, O. Just, H. T. Janka, and N. Stergioulas, Astrophys. J. Lett. **850** L34 (2017).

[13] E. F. Brown, A. Cumming, F. J. Fattoyev, C. Horowitz, D. Page, and S. Reddy, Phys. Rev. Lett. **120** 182701 (2018).

[14] J. M. Lattimer and M. Prakash, Phys. Rept. **442**, 109 (2007).

[15] B. Link, R. I. Epstein, and J. M. Lattimer, Phys. Rev. Lett. **83**, 3362-3365 (1999).

[16] N. Andersson, K. Glampedakis, W. Ho, and C. Espinoza, Phys. Rev. Lett. **109** 241103 (2012).

[17] D. G. Ravenhall and C. J. Pethick, Astrophys. J. **424** 846 (1994).

[18] F. Özel, T. Guver, and D. Psaltis, Astrophys. J. **693**, 1775 (2009).

[19] F. Özel and P. Freire, Ann. Rev. Astron. Astrophys. **54** 401 (2016).